Model dynamics and vertical collapse in decaying strongly stratified flows

Andrew J. Majda and Marcus J. Grote
Courant Institute of Mathematical Sciences, New York University, 251 Mercer Street, New York, New York 10012-1185

(Received 3 December 1996; accepted 5 June 1997)

Recent laboratory experiments with decaying strongly stratified grid turbulence at moderate Reynolds numbers reveal remarkable behavior. These experiments document the evolution of an initial sea of columnar dipole vortex pairs with dominant vertical vorticity to stratified ''pancake'' vortex sheets with dominant horizontal vorticity, together with a concurrent dominance of vertical dissipation of kinetic energy as compared with horizontal dissipation. Here we build exact solutions of the equations for low Froude number limiting dynamics, which capture basic qualitative features observed in the above experiments. Unlike the actual turbulent experiments, these exact solutions are laminar and do not involve a cascade of many scales in the horizontal. The exact solutions of the limiting dynamics involve a periodic array of dipole vortices in a weakly vertically sheared horizontal flow. The effect of finite Rossby numbers on the collapse of these exact solutions is also described here. At moderately large Rossby numbers, the effect of rotation is to inhibit the vertical collapse process. © *1997 American Institute of Physics.* [S1070-6631(97)01210-5]

I. INTRODUCTION

Recent laboratory observations[1–3] in the decaying wake region for stratified flows at long time display a remarkable transition from columnar vortex structures with dominant vertical vorticity to layered ''pancake'' vortex sheets with dominant horizontal vorticity. The dynamic process, which achieves this radical reorganization of the vorticity field, exhibits a concurrent dominance of vertical dissipation of kinetic energy as compared with horizontal dissipation.[1,3] Recent numerical simulations in idealized periodic geometry[4,5] with strongly stratified flows also exhibit a dominance of layered ''pancake'' vortex sheets with dominant horizontal vorticity.

The detailed experimental observations of Fincham *et al.*[1,3] are extremely revealing regarding the details of the collapse process mentioned above. These authors utilize high resolution Digital Particle Image Velocimetry (DPIV) in decaying stratified grid turbulence at large times (many buoyancy times) with Reynolds numbers varying from Re=760 to Re=12 000. The salient features observed in these experiments, especially at the lower Reynolds numbers, are the following.

A. Experimental observations

(A) The flow remains predominantly horizontal during the transition process with Froude number, $\mathrm{Fr}\ll 1$, and Richardson number, $\mathrm{Ri}\gg 1$. This condition for approximately horizontal flow means that $\vec{v}=\vec{v}_v+\vec{v}_H$, with $|\vec{v}_v| \ll |\vec{v}_H|$.

(B) At the initial stage, the flow looks like a ''complex sea'' of columnar dipole vortices in a weakly vertically sheared background flow. Thus, if $\vec{\omega}=(\vec{\omega}_H,\omega)$ is the three dimensional vorticity, at the initial stage there is much larger vertical vorticity

$$|\omega|\gg|\vec{\omega}_H|. \tag{1}$$

(C) At the later stages of the decay process, the flow field remains horizontal while the vorticity is mostly horizontal and arranged in vertically layered pancakes of horizontal vorticity with

$$|\vec{\omega}_H|\gg|\omega|. \tag{2}$$

(D) Consider the (horizontal) velocity field $\vec{v}_H(x,y,z,t)$ from (A). Fincham *et al.*[1,3] split the contributions to the dissipation of kinetic energy, $(d/dt)\frac{1}{2}\int|\vec{v}_H|_2^2=-\varepsilon$, into vertical and horizontal dissipation components,

$$\varepsilon=\varepsilon_{2D}+\varepsilon_z,$$
$$\text{with } \varepsilon_z=2\nu\overline{\left(\frac{\partial u}{\partial z}\right)^2}, \tag{3}$$

and ε_{2D} the horizontal plane turbulent dissipation. Here u denotes the x-component of the velocity. Then in the transition process from (B) to (C), the vertical dissipation of energy dominates over horizontal dissipation of kinetic energy, i.e.,

$$|\varepsilon_z|\gg|\varepsilon_{2D}|. \tag{4}$$

In (3), ε_z and ε_{2D}, are computed as a statistical average in the turbulent flow, as indicated by the overbar in (3) (see Fincham *et al.*[1] for the precise definition of ε_{2D}, although the notation is different). The interested reader can consult Figures 3, 4, and 8 in Fincham *et al.*[1] for quantitative confirmation of the features of the experimental observations, which we have outlined briefly in (A)–(D) above; in particular, typically 90% or more of the contribution to the dissipation arises from $|\varepsilon_z|$ as compared with $|\varepsilon_{2D}|$.

The development of simplified models which simultaneously capture the features in (A)–(D) in a qualitative fashion is an important theoretical issue. Here we develop exact solutions of simplified model dynamics which fulfill all of the requirements in (A)–(D). From (A) above, these flows are strongly stratified with $\mathrm{Fr}\ll 1$; thus, the starting point for the theoretical developments presented here are the simpli-

 1070-6631/97/9(10)/2932/9/$10.00

fied equations for low Froude number limiting dynamics, proposed on heuristic grounds by Riley *et al.*,[6] and recently derived in a general setting in the low Froude number limit with full mathematical rigor by Embid and Majda.[7,8]

The relevant properties of solutions of these equations for low Froude number limits are described briefly in Section II; in particular, general solutions of these equations automatically will satisfy (4), i.e., $|\varepsilon_z| \gg |\varepsilon_{2D}|$, provided that (1) is satisfied, i.e., $|\omega| \gg |\vec{\omega}_H|$. We end our discussion in Section II with an exact solution procedure for the limiting dynamics. In Section III, we apply this exact solution procedure for low Froude number limiting dynamics with initial data involving a periodic array of dipole vortices in a weakly vertically sheared horizontal flow to mimic (B). These exact solutions display vertical collapse in a fashion so that all three qualitative features in (B), (C), and (D) in the experimental observations occur simultaneously. The effect of finite Rossby numbers on the vertical collapse of these exact solutions is also described in Section III. Even at moderately large Rossby numbers, the effect of rotation is to inhibit the vertical collapse process.

II. LOW FROUDE NUMBER LIMITING DYNAMICS FOR STRONGLY STRATIFIED FLOWS

Motivated by the observations in (A) that the velocity field is nearly horizontal and the Froude number, Fr, satisfies $\mathrm{Fr} \ll 1$, here we utilize the simplified equations for the limiting dynamics.[6–8] We begin this section by briefly describing how these limiting dynamic equations emerge from the stably stratified rotating Boussinesq equations in the low Froude number limit. We also describe the non-dimensionalization used in these equations to make contact with the relevant length and time scales, which link the solutions of these equations qualitatively with those in the experiments.[1,3] The limiting dynamic equations involve no vertical velocity and only horizontal velocity components, $\vec{v}_H$, which can vary as functions of the vertical variable. This behavior is consistent with (A) in the experiments where $|\vec{v}_v| \ll |\vec{v}_H|$.

In Section II A, exact identities are developed for solutions of the limiting dynamics, which provide concise expressions for the dissipation of kinetic energy as a sum of horizontal and vertical components, the evolution of the three-dimensional vorticity field, and a quantitative link between these quantities, which guarantees within the limiting dynamics that the features described in (C) and (D) must occur simultaneously. In Section II B we develop an exact solution procedure for special solutions of the limiting dynamics, which we utilize in Section III to provide concrete examples where explicitly the features in (C) and (D) happen simultaneously. It is worth emphasizing here that, once one accepts the limiting dynamics as an approximation, all of the qualitative vertical collapse features described in Sections II A, II B, and III occur without any need for vertical overturning, since the vertical velocity component, w, always vanishes for these approximate dynamics.

We non-dimensionalize the stably stratified Boussinesq equations through a characteristic length scale, L, and a characteristic velocity U. We associate the characteristic length scale, L, with the typical separation distance between the initial columnar dipole vortices described in (B) above, while the velocity units are measured in the typical velocity magnitude U of the columnar dipole vortex pairs. Time is non-dimensionalized by the eddy turnover time, L/U, associated with this flow with corresponding Reynolds number $\mathrm{Re} = LU/\nu$. Besides these length and time scales, we utilize $\rho_b B$ for the scale of the density fluctuations, p for the pressure scale, and N for the constant buoyancy (Brunt-Väisälä) frequency characterizing the stable stratification, $N = (-(g/\rho_b)\partial_z \overline{\rho})^{1/2}$. With this choice of scales the non-dimensional form of the rotating Boussinesq equations is

$$\frac{\partial \vec{v}}{\partial t} + (\mathrm{Ro})^{-1} \vec{\eta} \times \vec{v} + \overline{P} \nabla \phi + \Pi^{-1} (\mathrm{Fr})^{-1} \rho \vec{e}_z + \vec{v} \cdot \nabla \vec{v} - (\mathrm{Re})^{-1} \Delta \vec{v} = 0,$$

$$\frac{\partial \rho}{\partial t} - \Pi (\mathrm{Fr})^{-1} w + \vec{v} \cdot \nabla \rho - (\mathrm{Re})^{-1} (\mathrm{Pr})^{-1} \Delta \rho = 0, \tag{5}$$

$$\mathrm{div}\ \vec{v} = 0,$$

where the non-dimensional numbers are

$$\mathrm{Ro} = \frac{U}{Lf} \text{ Rossby number}, \quad \mathrm{Fr} = \frac{U}{LN} \text{ Froude number},$$

$$\overline{P} = \frac{p}{\rho_b U^2} \text{ Euler number}, \quad \mathrm{Re} = \frac{\rho_b UL}{\mu} \text{ Reynolds number},$$

$$\mathrm{Pr} = \frac{\mu}{\rho_b D} \text{ Prandtl number}, \quad \Pi = \frac{NU}{gB}.$$

Here $\vec{v} = (\vec{v}_H, w)$ is the fluid velocity and ρ is the density fluctuation. For simplicity in exposition, we have assumed equal horizontal and vertical length scales in defining the Froude number.

The Froude number measures the ratio of the buoyancy time to the eddy turnover time. The actual experiments involve decaying flows so the Froude number starts at a small value and decreases in time during the observations. This motivates looking at simplified dynamic equations in the low Froude number limit to qualitatively capture some basic features of the experiments. To achieve this low Froude number limit, we utilize the balance of buoyancy fluctuations given by

$$\mathrm{Fr} = \varepsilon, \quad \overline{P} = 1, \ \Pi = 1, \tag{6}$$

in the non-dimensional Boussinesq equations.

Low Froude number limiting dynamics. The equations for the (slow) dynamics, which have been derived rigorously[7] from the stratified rotating Boussinesq equations in the above low Froude number limit with $\varepsilon \to 0$, are given by

$$\frac{\partial \vec{v}_H}{\partial t} + \vec{v}_H \cdot \nabla_H \vec{v}_H + (\mathrm{Ro})^{-1} \vec{v}_H^{\perp} + \nabla_H \phi$$

$$= (\mathrm{Re})^{-1} \Delta_H \vec{v}_H + (\mathrm{Re})^{-1} \frac{\partial^2 \vec{v}_H}{\partial z^2},$$

$$\mathrm{div}_H \ \vec{v}_H = 0, \tag{7}$$

$$w \equiv 0,$$

$$\frac{\partial \rho}{\partial t} = (\mathrm{Re})^{-1} (\mathrm{Pr})^{-1} \frac{\partial^2 \rho}{\partial z^2},$$

where $\vec{v}_H^{\perp} = (-v_2, v_1)$. In the slow dynamics equations the velocity and the density are decoupled. Consistent with (A), the fluid is strongly stratified with zero vertical velocity w and density ρ that only changes in the vertical direction. The different horizontal layers of fluid exchange momentum through diffusion in the vertical direction. For the special case with $\mathrm{Ro} = +\infty$, the equations in (7) have been proposed earlier on heuristic grounds by Riley *et al.*[6] In (7) we assume the flow is 2π-periodic in all three directions for simplicity. With the non-dimensionalization of the spatial scales described above, we consider a vortex dipole pair on this unit length scale with unit velocity in a weak vertical shear in this periodic geometry as a qualitative model for the initial data mimicing (B) from the experiments. This motivates the initial data for the exact solutions described below in Sections II A and III.

A. Exact vorticity and dissipation formulas for the limiting dynamics

We begin with the dissipation of kinetic energy, $E(t) = \frac{1}{2} \|\vec{v}_H\|_2^2$, where for any function, f, $\|f\|_2^2 = \int f^2 dxdydz$. By multiplying the first equation in (7) by $\vec{v}_H$ and integrating by parts, it is straightforward to derive the identity

$$\frac{d}{dt} E = -(\mathrm{Re})^{-1} \left\| \frac{\partial \vec{v}_H}{\partial z} \right\|_2^2 - (\mathrm{Re})^{-1} \|\nabla_H \vec{v}_H\|_2^2 \equiv \varepsilon_z + \varepsilon_{2D}. \tag{8}$$

The experimental evidence in (B), (C), and (D) shows that the vertical dissipation of kinetic energy ε_z grows in time and dominates the horizontal dissipation ε_{2D}. Thus to mimic the experiments, we need to build solutions of the limiting dynamics which satisfy

$$\left\| \frac{\partial \vec{v}_H}{\partial z} \right\|_2^2 \gg \|\nabla_H \vec{v}_H\|_2^2,$$

as time evolves.

The horizontal velocity field, $\vec{v}_H$, satisfying the equations in (7), has the unique decomposition

$$\vec{v}_H = \vec{V}_H + \nabla_H^{\perp} \psi, \tag{9}$$

where $\vec{V}_H(z,t) = \int \vec{v}_H(x,y,z,t) dxdy$ is a vertically sheared periodic flow and ψ is the horizontal stream function with $\nabla_H^{\perp} \psi = (-\partial_y \psi, \partial_x \psi, 0)$. Although the velocity field is purely horizontal in the limiting dynamics, the total vorticity $\vec{\omega}$ is three-dimensional and

$$\vec{\omega} = \mathrm{curl} \begin{pmatrix} \vec{V}_H + \nabla_H^{\perp} \psi \\ 0 \end{pmatrix} = \begin{pmatrix} \partial_z \vec{V}_H^{\perp} \\ 0 \end{pmatrix} + \begin{pmatrix} \vec{\omega}_H' \\ \omega \end{pmatrix}, \tag{10}$$

where ω and $\vec{\omega}_H'$ are given by

$$\omega = \Delta_H \psi, \quad \vec{\omega}_H' = \frac{\partial}{\partial z} \nabla_H \psi. \tag{11}$$

Our goal is to construct elementary exact solutions in the low Froude number limit that exhibit the key features outlined in (B), (C), and (D) of the introduction. We note that some remarkable elementary identities guarantee that the two effects in (C) and (D) must occur simultaneously within the context of limiting dynamics. Indeed, since

$$\frac{\partial \vec{v}_H}{\partial z} = \frac{\partial \vec{V}_H}{\partial z} + \frac{\partial}{\partial z} \nabla_H^{\perp} \psi, \tag{12}$$

we infer using (10) that

$$\left| \frac{\partial \vec{v}_H}{\partial z} \right| = \left| \vec{\omega}_H' + \frac{\partial \vec{V}_H^{\perp}}{\partial z} \right| \quad \text{pointwise.} \tag{13}$$

We will see below that $|\partial_z \vec{V}_H^{\perp}|$ cannot grow in time, since it satisfies the linear convection-diffusion equation in (14). Thus, growth of $|\vec{\omega}_H'|$ implies the growth of $|\partial_z \vec{v}_H|$ pointwise.

Next, we derive the vorticity-stream form of the equations for the limiting slow dynamics in (7). We recall the decomposition $\vec{v}_H = \vec{V}_H(z,t) + \nabla_H^{\perp} \psi$ from (7) and also from (11) that the vertical component of the vorticity is related to the stream function ψ by $\omega = \Delta_H \psi$. Therefore, computing the horizontal average of (7) and the vertical component of the vorticity from the curl of the horizontal momentum equations in the limiting dynamics in (7) yields the following:

Vorticity-stream form of the limiting dynamics for low Froude and finite Rossby numbers. The horizontal velocity is $\vec{v}_H = \vec{V}_H + \nabla_H^{\perp} \psi$, where the vertical shear $\vec{V}_H$ satisfies

$$\frac{\partial \vec{V}_H}{\partial t} + (\mathrm{Ro})^{-1} \vec{V}_H^{\perp} = (\mathrm{Re})^{-1} \frac{\partial^2}{\partial z^2} \vec{V}_H. \tag{14}$$

The vertical vorticity ω and the stream function ψ satisfy the vorticity-stream equations

$$\frac{\partial \omega}{\partial t} + \vec{V}_H \cdot \nabla_H \omega + J_H(\psi, \omega) = (\mathrm{Re})^{-1} \Delta_H \omega + (\mathrm{Re})^{-1} \frac{\partial^2 \omega}{\partial z^2},$$

$$\Delta_H \psi = \omega, \tag{15}$$

where $J_H(\psi, \omega) = \nabla_H^{\perp} \psi \cdot \nabla_H \omega$ is the Jacobian of ψ and ω in the horizontal variables.

The limiting dynamic equations at low Froude number also include the effects of the slow vortical modes described in (7) on the (fast) internal gravity waves as well as three-wave resonances among internal gravity waves.[7] Since the internal gravity waves are primarily radiated to the walls of

the tank and dissipated there in laboratory experiments, we ignore the fast wave dynamics in our discussion here for simplicity in exposition; the theory presented by Embid and Majda[7] guarantees that such a procedure is self-consistent for the periodic geometries considered here. Also we ignore the density equation from (7), since it has a passive role in the leading order slow dynamics.

Next, we study the mechanism for the growth of $|\vec{\omega}_H'|$ in time. From (11), we see that

$$\vec{\omega}_H' = \nabla_H \Delta_H^{-1}\left(\frac{\partial \omega}{\partial z}\right). \tag{16}$$

Thus growth in $\partial_z \omega$ implies growth in the magnitude of $\vec{\omega}_H'$. Although $|\omega|$ cannot grow in time, $\partial_z \omega$ can grow through enhanced turbulent diffusion driven by the shear $\vec{V}_H(z,t)$ in (14). This physical mechanism is well-known intuitively, but we shall now build exact solutions that demonstrate this.

B. An exact solution procedure

We build exact solutions of the limiting dynamics in (14) and (15), which exhibit the two simultaneous mechanisms (C) and (D) from the introduction via equation (16), where ω is computed from the solutions of (14) and (15).

From equation (14) it is clear that the vertical shear component $\vec{V}_H$ evolves independently of the horizontal velocity $\nabla_H^{\perp}\psi$. In fact, the dynamics of $\vec{V}_H$ are described by a linear equation with constant coefficients, which we can solve immediately via Fourier series. Let $R(t)$ be the rotation matrix

$$R(t) = \begin{pmatrix} \cos(\mathrm{Ro})^{-1}t & \sin(\mathrm{Ro})^{-1}t \\ -\sin(\mathrm{Ro})^{-1}t & \cos(\mathrm{Ro})^{-1}t \end{pmatrix}. \tag{17}$$

Then the solution of (14) is

$$\vec{V}_H(z,t) = \sum_{k=-\infty}^{\infty} e^{ikz} e^{-(\mathrm{Re})^{-1}k^2 t} R(t) \widehat{\vec{V}_H}(k). \tag{18}$$

From (18) we see that $\vec{V}_H(z,t)$ represents a time decaying vertical shear flow, which rotates with uniform angular velocity $(\mathrm{Ro})^{-1}$. We note that if $(\mathrm{Ro})^{-1}=0$, then $R(t)=I$.

Next, we construct *special exact solutions* of (15). We select a *single fixed* energy shell $\Lambda \geqslant 1$ and consider a superposition of *horizontal* Fourier modes $\vec{k}_H=(k_1,k_2)$, k_1 and k_2 integers, within that shell,

$$\psi(x,y,z,t) = \sum_{|\vec{k}_H^j|^2=\Lambda} A_j(z,t) e^{i\vec{k}_H^j \cdot \vec{x}_H} e^{-(\mathrm{Re})^{-1}\Lambda t}. \tag{19}$$

To ensure that ψ is real, we must include for each Fourier component A_j its complex conjugate $A_i = A_j^*$, with $\vec{k}_H^i = -\vec{k}_H^j$. With this particular choice of ψ, we immediately derive the two formulas

$$\begin{aligned} &\omega = \Delta_H \psi = -\Lambda \psi, \\ &\vec{\omega}_H' = \nabla_H \frac{\partial}{\partial z}(-\Lambda^{-1}\omega) = -\Lambda^{-1}\left(\nabla_H \frac{\partial \omega}{\partial z}\right). \end{aligned} \tag{20}$$

The first property in (20) causes the nonlinear term in (15), $J_H(\psi,\omega)$, to vanish so that (15) becomes a *linear* advection-diffusion equation; moreover, this condition is self-consistently satisfied by the solution of the advection-diffusion equation as time evolves. By introducing (19) into (15), we see that the complex amplitudes $A_j(z,t)$ solve the linear equation

$$\begin{aligned} &\frac{\partial}{\partial t} A_j(z,t) + i\vec{k}_H^j \cdot \vec{V}_H(z,t) A_j(z,t) = (\mathrm{Re})^{-1} \frac{\partial^2}{\partial z^2} A_j(z,t), \\ &|\vec{k}_H^j|^2 = \Lambda, \end{aligned} \tag{21}$$

for some given initial conditions $A_j(z,t) = A_j^0(z)$ at $t=0$.

In the next section, we process these exact solutions with appropriate initial data to display simultaneously all of the qualitative features (B)–(D) observed in the experiments, even though these elementary exact solutions do not involve a cascade of many scales. The initial data we choose corresponds to a large scale dipole vortex with $|\vec{k}_H^j|^2 = 1$, consistent with our non-dimensionalization described earlier. We solve the finite number of linear equations in (21) for the amplitudes $A_j(z,t)$ straightforwardly through second order accurate time-splitting via fractional steps. The spatial z-derivatives are computed through Fast Fourier Transform in standard fashion. We found that 64 mesh points in z with a time step $\Delta t = 0.1$ guaranteed accuracy within $O(10^{-5})$ for all the solutions reported in the next section.

III. EXACT SOLUTIONS EXHIBITING VERTICAL COLLAPSE

In all of the solutions presented in this section utilizing the exact solution procedure in (18)–(21), for initial data, we use the periodic dipole flow configuration with stream function

$$\psi(x,y,z,0) = \sin(x) + \sin(y). \tag{22}$$

The initial condition for the background vertically sheared motion, $\vec{V}_H(z,t)$, is given by

$$\vec{V}_H(z,0) = \begin{pmatrix} V_{\max}\sin(z) \\ 0 \end{pmatrix}. \tag{23}$$

The constant $V_{\max}$ controls the strength of the shear; typically, we set $V_{\max}=0.1$ so that the magnitude of the vertical shear is 5% of the size of the vorticity magnitude in the dipole. Clearly, these initial data mimic the experimentally observed initial stage described in (B) from the introduction, involving a sea of dipole vortices in a weakly vertically sheared background flow. Below, we also vary the strength of the vertical shear through the moderate amplitudes for $V_{\max}$ between 0.05 and 0.5.

A. Vertical collapse dynamics at low Froude numbers

Here we show that the dynamical evolution of the exact solutions from (18)–(21) with the initial data from (22) qualitatively captures all of the features from the experiments outlined in (C) and (D) from Section I.

At Reynolds number, $\mathrm{Re}=1000$, we set $V_{\max}=0.1$ in (23) for the initial data and suppress rotation with

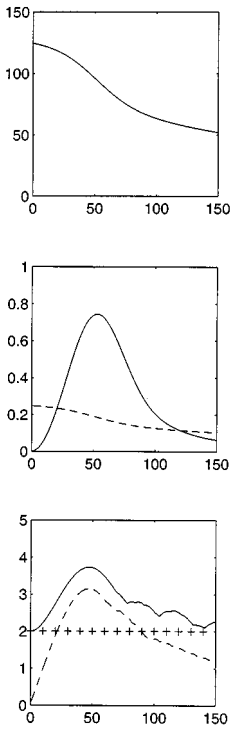

FIG. 1. The exact solutions described in Section III without rotation, $(\mathrm{Ro})^{-1}=0$, with Reynolds number $\mathrm{Re}=1000$, and with maximal vertical shear strength $V_{\max}=0.1$ are monitored versus time: the total energy [top]; the horizontal and vertical energy dissipation rates, ε_{2D} (dashed) and ε_z (plain) [middle]; the maximal horizontal vorticity, $\vec{\omega}_H$ (dashed), the maximal vertical vorticity, $\vec{\omega}_z$ (plus), and the maximal total vorticity, $\vec{\omega}$ (plain) [bottom].

$(\mathrm{Ro})^{-1}=0$. In Figure 1, we graph the energy decay as a function of time in the first frame, while the second frame follows the horizontal and vertical dissipation rate, defined earlier in (8). The third frame in Figure 1 follows the vertical, horizontal, and total vorticity amplitudes as a function of time. Clearly by time $t=50$, the vertical dissipation rate swamps the horizontal dissipation rate and contributes nearly 80% of the dissipation. Also, simultaneously, the horizontal vorticity maximum dominates the vertical vorticity maximum. These two graphs give strong evidence that both effects from (C) and (D) in the introduction are occurring simultaneously in the exact solutions from (18)–(21) with the above initial data.

To further corroborate the behavior of these exact solutions as a qualitative model for the process in (C) and (D), we present snapshots of the corresponding vorticity field at time $t=0,10,20,30,40,50$ in Figure 2(a). Here we plot the set of points where the vorticity is within 90% of its maximum. Clearly at time $t=0$, we see essentially the columnar vortex dipole pair since the vertical shear is very weak. The dynamic formation of the layered pancake sheets with large horizontal vorticity is already evident at times $t=20,30$ and continues in time until $t=50$. We also note that the initial breakup of the vertical vortex tubes at $t=10$ occurs, as one would expect, in the vicinity of the locations at $z=0,\pi,2\pi$, where the vertical shear has its maximum gradient so that the viscous dissipation is more effective. In Figure 2(b) we display the vorticity field at two different heights, $z=\pi/2$ and $z=2\pi$, at times $t=0,20,50$. These snapshots of the vorticity clearly demonstrate the strong increase with time in the horizontal component of the vorticity at locations of maximal gradient in the vertical shear.

The graphical data just presented in Figures 1 and 2 demonstrate that the exact solutions of the low Froude number limiting dynamics described in Section II are a qualitative model for all of the features observed experimentally and summarized in (B), (C), and (D) of the introduction. We emphasize that no vertical overturning was utilized in building these solutions.

To see the effect of Reynolds number and the maximum of the vertical shear on the vertical dissipation, we varied these parameters systematically for the exact solutions in (18)–(21), with the initial data in (22) and (23) for Reynolds numbers, $500\leqslant \mathrm{Re}\leqslant 5000$ and $V_{\max}$ with $0.05\leqslant V_{\max}\leqslant 0.5$. In Figure 3 we plot the vertical dissipation as a percentage of total dissipation at the temporal maximum of vertical dissipation as the parameters Re and $V_{\max}$ vary. Note that even with $V_{\max}=0.05$, 85% of the dissipation rate is vertical at $\mathrm{Re}=5000$. Not surprisingly, the larger values of $V_{\max}$ have even more efficient vertical dissipation.

B. Vertical collapse at finite Rossby numbers

Here we indicate the effect of rotation on the vertical collapse of the exact solutions which we have just described in Section III A. First, we use $\mathrm{Re}=1000$ and the same initial data as in Figures 1 and 2 with $V_{\max}=0.1$, but utilize a Rossby number, $\mathrm{Ro}=10$ in the exact solution procedure from (18)–(21). Figure 4 presents the energy decay, the horizontal and vertical dissipation, and the vertical, horizontal, and total vorticity amplitude as time evolves in this situation with $\mathrm{Ro}=10$. Both the vertical dissipation and the horizontal vorticity are drastically reduced in time even at the high Rossby number, $\mathrm{Ro}=10$, as the reader can easily verify by comparing Figure 4 with Figure 1. The decaying oscillations in both the vertical dissipation and the horizontal vorticity correlate precisely with the rotation period.

In Figure 5, we evaluate the same time histories as in Figure 4, but raise $V_{\max}$ to $V_{\max}=0.175$ while keeping $\mathrm{Re}=1000$ and $\mathrm{Ro}=10$. With this higher shear strength, the vertical dissipation is more than twice the horizontal dissipation at time $t\simeq 25$ with a corresponding growth in horizontal vorticity. Both of these examples demonstrate that even a moderately high Rossby number, i.e., moderate rotation, has the effect of decorrelating the action of sufficiently weak horizontal shears.

Is the vertical dissipation rate in the exact solutions a monotone function of Rossby number for fixed initial data from (22) and (23) at a given Reynolds number? From the data just presented in Figures 4 and 5, the reader might suspect that the answer is yes. However, instead, we find a narrow range of large Rossby numbers where finite rotation effects can actually enhance vertical dissipation in contrast to the data in Figures 4 and 5 at fixed Rossby number,

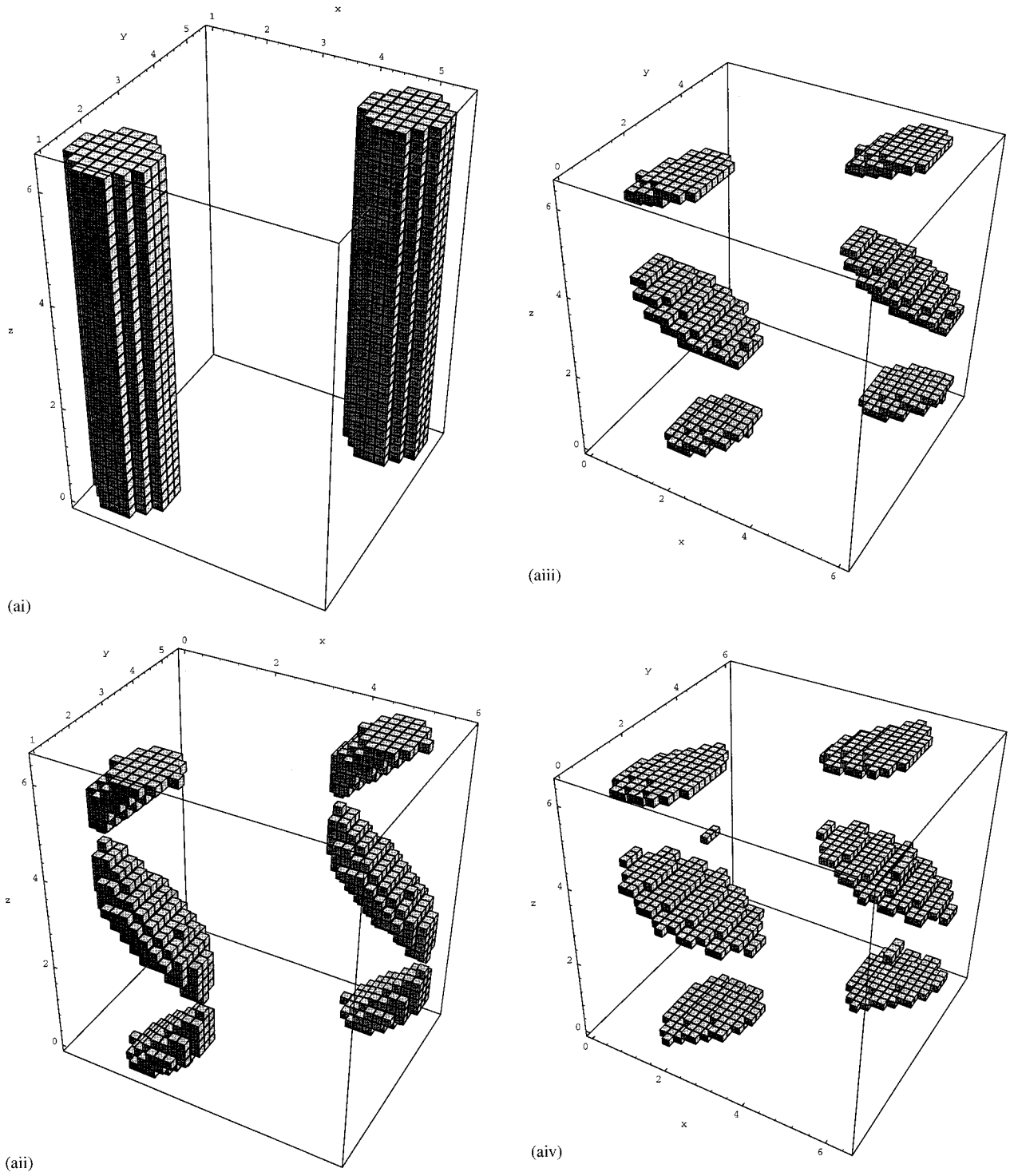

FIG. 2. The exact solutions described in Section III without rotation, $(\mathrm{Ro})^{-1}=0$, with Reynolds number $\mathrm{Re}=1000$, and with maximal vertical shear strength $V_{\max}=0.1$. Part (a): the locations where the total vorticity $|\vec{\omega}|$ is within 90% of its maximum are shown at various times (i) $t=0$, (ii) $t=10$, (iii) $t=20$, (iv) $t=30$, (v) $t=40$, (vi) $t=50$. Part (b): snapshots of the vorticity field at two different heights; $z=\pi/2$ and $z=2\pi$, are shown at various times: (i) $t=0$, (ii) $t=20$, (iii) $t=50$. The amplitude of the vorticity is scaled at 25% of its actual strength.

$\mathrm{Ro}=10$. In Figure 6 we plot the vertical dissipation as a percentage of total dissipation at the temporal maximum of vertical dissipation as the parameters Re and Ro vary for the fixed initial data in (22) and (23) with $V_{\max}=0.1$. For fixed Reynolds number, the maximum horizontal dissipation with varying Rossby number occurs at $\mathrm{Ro}\simeq 50$ for $\mathrm{Re}\simeq 1000$. The efficiency of dissipation is enhanced at all Reynolds numbers due to the time-dependent motion of the velocity field at relatively high Rossby numbers. However, the efficiency of vertical dissipation diminishes very rapidly as the Rossby number decreases. Similar behavior occurs at the larger Reynolds numbers up to 5000 but is not depicted here.

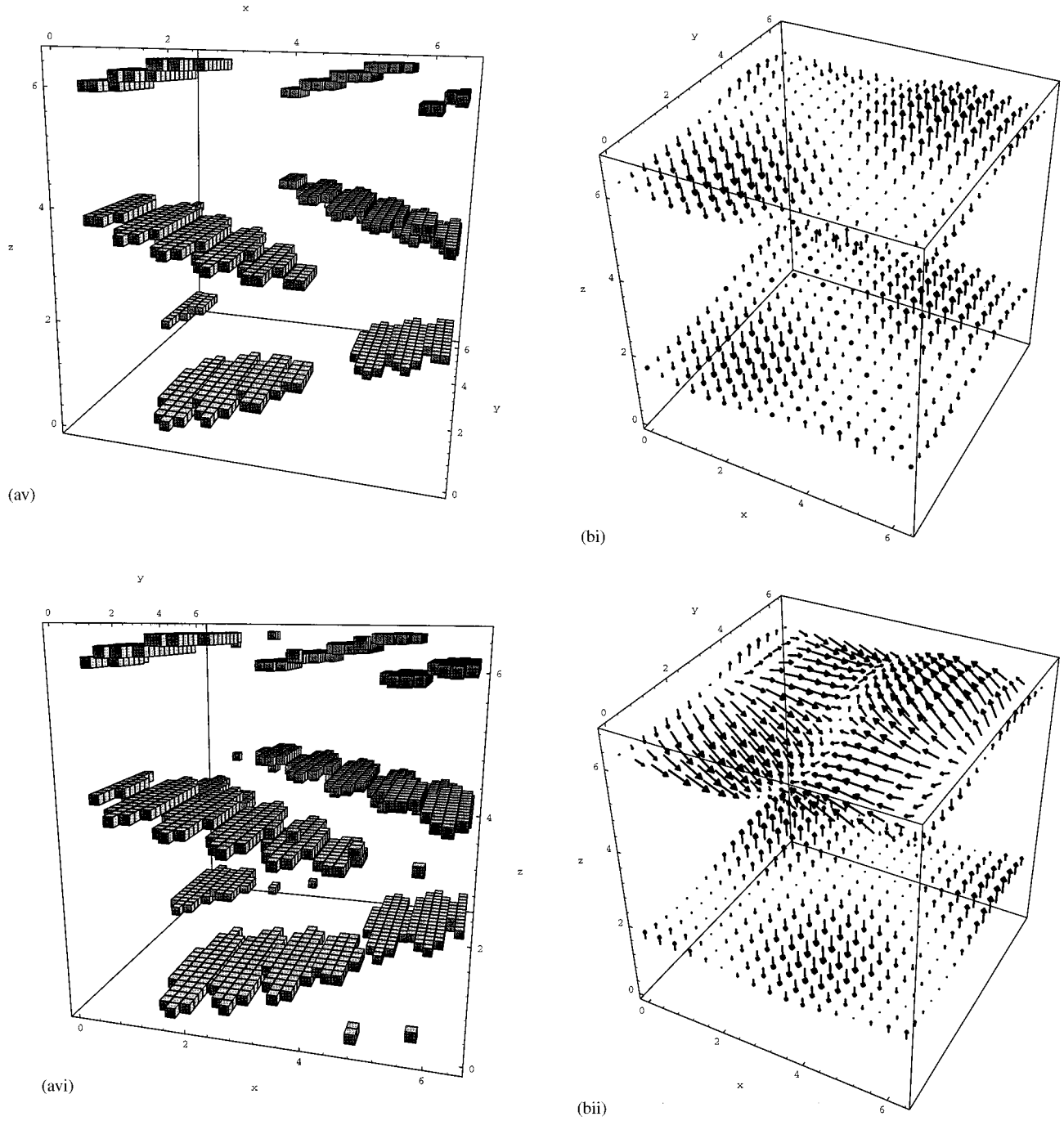

FIG. 2. (*Continued.*)

IV. CONCLUDING DISCUSSION

Motivated by remarkable experimental observations[1,3] in decaying stratified flows, we have presented exact solutions of the equations for low Froude number limiting dynamics,[6–8] which qualitatively model key features of the observed vertical collapse. The features include, in a purely horizontal evolving flow, a temporal transition from nearly columnar dipole vortices in a weak vertical shear to vertically layered pancake vortex sheets with dominant horizontal vorticity; this radical geometric change in vortex structure is accompanied by concurrent dominance of vertical dissipation compared with horizontal dissipation in these solutions. The exact solutions presented in Section II and developed in Section III are capable of capturing all of these facets simultaneously. The effects of moderate rotation on these exact solutions have also been documented. In general, moderate Rossby numbers inhibit both vertical dissipation and horizontal vorticity production in these exact solutions although, surprisingly, there is a narrow window of rather large Rossby numbers where rotation enhances these effects.

However, these exact laminar solutions probably do not model the actual turbulent experiments in quantitative fash-

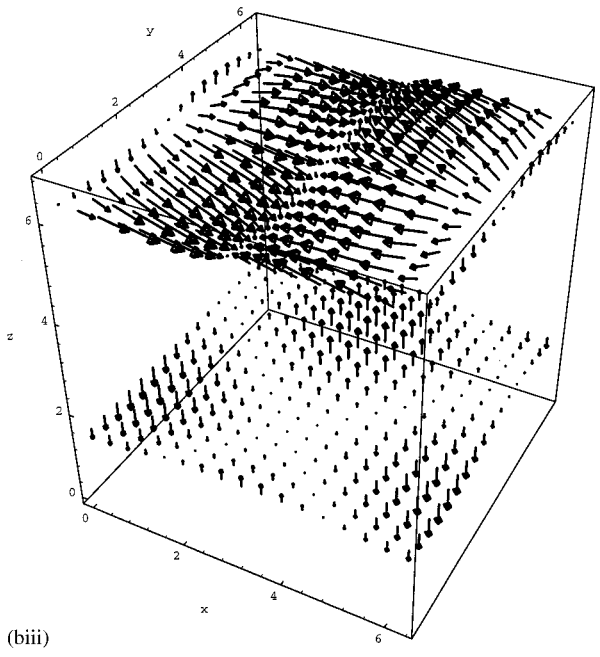

(biii)

FIG. 2. (*Continued.*)

ion, since the experiments involve a significant cascade to small scales in horizontal and vertical wave number. In contrast the exact solutions involve dissipation on the same horizontal scales of motion as the large scale motion, so that quantitative agreement with experiments is only possible at lower Reynolds numbers than the actual experiments in Fincham *et al.*[1]

While the exact solutions presented here qualitatively model a number of interesting dynamical features, these solutions are almost certainly dynamically unstable since by the construction (18)–(21) of Section II, each amplitude coefficient, $A_j(z,t)$, from (21) moves independently. Nevertheless, it is interesting to perturb these solutions and include

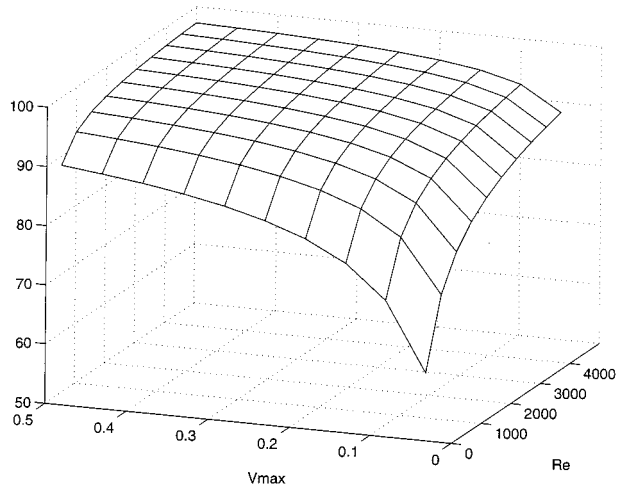

FIG. 3. For the exact solutions described in Section III without rotation, $(\mathrm{Ro})^{-1}=0$, the vertical energy dissipation, ε_z, as a percentage of total dissipation, ε, is shown at the temporal maximum at vertical dissipation, as the Reynolds number Re and the vertical shear strength $V_{\max}$ vary.

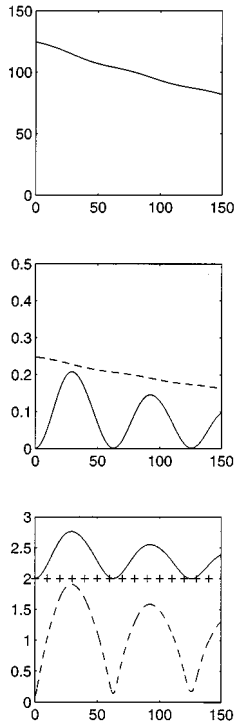

FIG. 4. The exact solutions described in Section III with rotation, $(\mathrm{Ro})=10$, with Reynolds number $\mathrm{Re}=1000$, and with maximal vertical shear strength $V_{\max}=0.1$ are monitored versus time: the total energy [top]; the horizontal and vertical energy dissipation rates, ε_{2D} (dashed) and ε_z (plain) [middle]; the maximal horizontal vorticity, $\vec{\omega}_H$ (dashed), the maximal vertical vorticity, $\vec{\omega}_z$ (plus), and the maximal total vorticity, $\vec{\omega}$ (plain) [bottom].

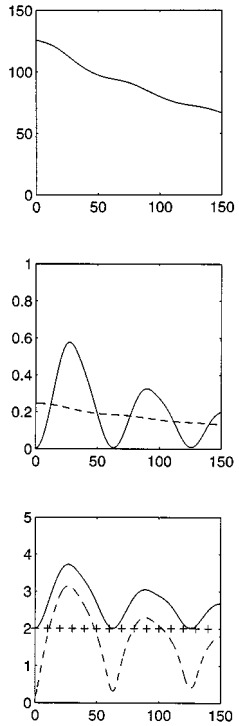

FIG. 5. The exact solutions described in Section III with rotation, $(\mathrm{Ro})=10$, and with increased maximal vertical shear strength $V_{\max}=0.175$ are monitored versus time: the total energy [top]; the horizontal and vertical energy dissipation rates, ε_{2D} (dashed) and ε_z (plain) [middle]; the maximal horizontal vorticity, $\vec{\omega}_H$ (dashed), the maximal vertical vorticity, $\vec{\omega}_z$ (plus), and the maximal total vorticity, $\vec{\omega}$ (plain) [bottom].

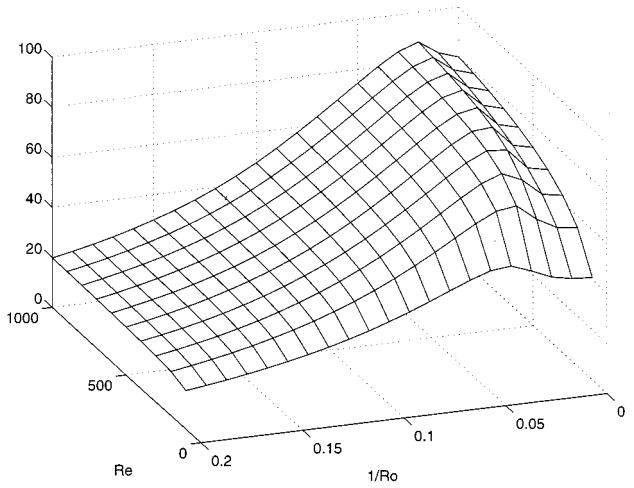

FIG. 6. For the exact solutions described in Section III with fixed vertical shear strength, $V_{\max}=0.1$, the vertical energy dissipation, ε_z, as a percentage of total dissipation, ε, is shown at the temporal maximum of vertical dissipation, as the Reynolds number Re and the inverse Rossby number $(\mathrm{Ro})^{-1}$ vary.

the effect of gravity waves at small finite Froude number and fixed Rossby number via controlled numerical experiments in periodic geometry. Also, the rough mathematical requirements[7,8] for the validity of these solutions at a finite small Froude number would impose the relation $\mathrm{Re} \leqslant O((\mathrm{Fr}^{-1}))$, with $\mathrm{Fr} \ll 1$, and it is useful to investigate whether these conditions actually are needed. As regards the collapse dynamics, it is interesting to develop other exact solutions which also incorporate large scale horizontal rotation and strain.[9] The authors are pursuing all of these issues and will report on the results in the near future.

ACKNOWLEDGMENTS

Andrew Majda's research is partially supported by grants NSF DMS-9596102-001, NSF DMS-9625795, ONR N00014-96-0043, and ARO DAAH04-95-1-0345. Marcus Grote has been supported as a postdoctoral fellow at the Courant Institute through ARO DAAH04-95-1-0345.

[1] A. M. Fincham, T. Maxworthy, and G. R. Spedding, ''The horizontal and vertical structure of the vorticity field in freely-decaying stratified grid turbulence,'' Dyn. Atmos. Oceans **23**, 155 (1996).
[2] G. R. Spedding, F. K. Browand, and A. M. Fincham, ''Turbulence, similarity scaling and vortex geometry in the wake of a towed sphere in a stably stratified fluid,'' J. Fluid Mech. **314**, 53 (1996).
[3] T. Maxworthy, personal communication from lecture at NCAR Workshop on Strongly Stratified Rotating Turbulence, July 1996.
[4] J. R. Herring and O. Metais, ''Numerical experiments in forced stably stratified turbulence,'' J. Fluid Mech. **202**, 97 (1989).
[5] Y. Kimura and J. Herring, ''Stratified turbulence: Structural issues and turbulent diffusion,'' preprint, July 1996.
[6] J. J. Riley, R. W. Metcalfe, and M. A. Weissman, ''Direct numerical simulation of homogenous turbulence in density-stratified fluids,'' in *Proceedings of the AIP Conference on Nonlinear Properties of Internal Waves*, edited by B. J. West (AIP, New York, 1981), pp. 79–112.
[7] P. Embid and A. J. Majda, ''Low Froude number limiting dynamics for stably stratified flow with small or fixed Rossby numbers,'' Geophys. Astro. Fluid Dyn. (in press).
[8] P. F. Embid and A. J. Majda, ''Averaging over fast gravity waves for geophysical flows with arbitrary potential vorticity,'' Comm. Part. Diff. Eqs. **21**, 619 (1996).
[9] A. J. Majda and M. J. Grote, ''The effect of large scale strain and rotation on vertical collapse in decaying strongly stratified flows,'' in preparation.